Effect of Grid-connected SOFC Power Generation on Power Systems Small-Signal Stability

Wang, H. (2012). Effect of Grid-connected SOFC Power Generation on Power Systems Small-Signal Stability. IET Renewable Power Generation, 6, 24-34.

Published in:
IET Renewable Power Generation

Techset Composition Ltd, Salisbury
Doc: H:/lee/RPG/Articles/Pagination/RPG20100024.3d

Published in IET Renewable Power Generation
Received on 31st January 2009
Revised on 27th March 2011
doi: 10.1049/iet-rpg.2010.0024

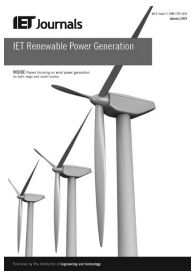

ISSN 1752-1416

Effect of grid-connected solid oxide fuel cell power generation on power systems small-signal stability

W. Du[1,2] *H.F. Wang*[2] *X.F. Zhang*[1] *L.Y. Xiao*[3]

[1]*School of Electrical Engineering, Southeast University, Nanjing, People's Republic of China*
[2]*School of Electronics, Electrical Engineering and Computer Science, Queen's University of Belfast, Belfast, UK*
[3]*Institute of Electrical Engineering, Chinese Academy of Science, Beijing, People's Republic of China*
Q1 *E-mail: ddwenjuan@googlemail.com*

Abstract: This study investigates one of the most fundamental issues of integrating fuel cell (FC) generation into power systems – its effect on power system small-signal stability when it operates jointly with conventional power generation. The study first presents a comprehensive mathematical model of the solid oxide fuel cell (SOFC) power plant integrated with the single-machine infinite-bus power system. Based on the model, conventional damping torque analysis is carried out to study the effect of SOFC power generation on power system small-signal stability. The analysis concludes that system small-signal stability can be affected either positively or negatively by the SOFC power plant when system operating conditions change. Two examples of power systems with gird-connected SOFC power plants are presented. Small-signal stability of the first example of single-machine power system was examined when the power system operated at different load conditions and levels of mixtures of conventional and FC power generation. The second example is a four-machine two-area power system where the power supplied by the gird-connected SOFC power plant is variable. Results of simulation using full non-linear model of the power systems and the SOFC power plants are given. All the results from the example power systems confirm and further demonstrate the analysis presented and conclusions obtained.

1 Introduction

Fuel cell (FC) power generation is of low to zero emission with high efficiency (35–60%) and is classified into various groups according to the electrolyte types, among which the high-temperature solid oxide fuel cell (SOFC) is considered to have the most significant potential as the future grid-connected clean power generation source [1, 2]. With the fast advancement of FC generation technology, it is foreseen that in near future, grid-connected operation of large-scale FC generation will affect not only the distribution networks but also transmission grid and the rest of the generators. The effect of large-scale FC power generation on the security and stability of future power system must be investigated carefully [3–7], including power system small-signal stability, which is the subject of this paper. However, so far there have been very few publications about the impact of penetration of FC generation on power system stability. Dynamic model of FC generation and its integration into power systems are discussed in [3–5]. Pioneering work presented in [6, 7] contributes to the very foundation of the research topic – FC dynamic model and its impact on power system control and stability.

The objective of this paper is to gain a clear understanding on and deep insight into the effect of FC generation on power system small-signal stability when it operates jointly with conventional power generation. Power system small-signal stability is predominantly affected by conventional generation, that is, the performance of synchronous generators. This paper investigates that when the penetration of FC generation reaches the level of conventional generation in a power system, how and why the system small-signal stability is influenced. As the first step in the study, this paper considers a simple single-machine infinite-bus power system integrated with a SOFC power plant. The capacity of the SOFC power plant is assumed to be comparable to that of the synchronous generator in the power system. This can be the case that the SOFC power plant could represent the effect of a congregation of many FC generation units or that it is a single FC generation unit in a future power system. In this paper, a conventional and effective method of damping torque analysis [8–10] is used to examine the damping torque contribution from the SOFC power plant to the electromechanical oscillation loop of the synchronous generator. Theoretical analysis in this paper indicates that the SOFC power plant can contribute either positive or negative damping to power system oscillations. The reason is that the damping torque contribution from the SOFC power plant changes from negative to positive damping torque when system operating conditions change. It is revealed that the decisive factor affecting the variations of damping torque contribution from the SOFC power plant is the angle between the ac voltage at the terminal of dc–ac converter of the SOFC power plant and the *d*-axis of the

synchronous generator. There exists a critical angle when the damping torque contribution from the SOFC power plant changes sign. Hence this paper proposes that the critical angle is defined as the stability limit of the operation of the SOFC power plant, as far as the small-signal stability of the single-machine infinite-bus power system is concerned.

In order to demonstrate the possibility to extend the analytical conclusions obtained in the paper to the more complex case of a multi-machine power system, a second example of a four-machine two-area power system with a grid-connected SOFC power plant is presented. The SOFC power plant adopts a different control scheme to that used for the study of the single-machine infinite-bus power system in the paper. Results of modal computation and simulation show that the effect of the SOFC power generation on the small-signal stability of the example power system changes with the variation of the operating conditions of the SOFC power plant and the conclusion is obtained in the paper for the single-machine infinite-bus power system.

2 Modelling a SOFC power plant into a power system

Fig. 1 shows the configuration of a SOFC power plant connected to a simple single-machine infinite-bus power system. X_{ts}, X_{sb}, X_{cs} and X_{fs} denote the equivalent reactance of transformers or/and transmission line. General mathematical model of the synchronous generator can be written as $\dot{\boldsymbol{X}}_g = \boldsymbol{F}(\boldsymbol{X}_g, \bar{I}_{ts})$, where $\boldsymbol{X}_g$ is the state variable vector associated with generator dynamics (see (1) below) and $\bar{I}_{ts}$ is the interface variable between the generator and rest of the system. In d–q coordinate of the generator, $\bar{I}_{ts}$ can be expressed by its d and q component, i_{tsd} and i_{tsq}, respectively. In this paper, the following generator model is used, which is sufficient for the study of power system small-signal stability [8]

$$\begin{aligned}
\dot{\delta} &= \omega_o(\omega - 1) \\
\dot{\omega} &= \frac{1}{M}[P_m - P_t - D(\omega - 1)] \\
\dot{E}'_q &= \frac{1}{T'_{d0}}(-E_q + E_{fd}) \\
\dot{E}'_{fd} &= -\frac{1}{T_A}E'_{fd} + \frac{K_A}{T_A}(V_{tref} - V_t)
\end{aligned} \tag{1}$$

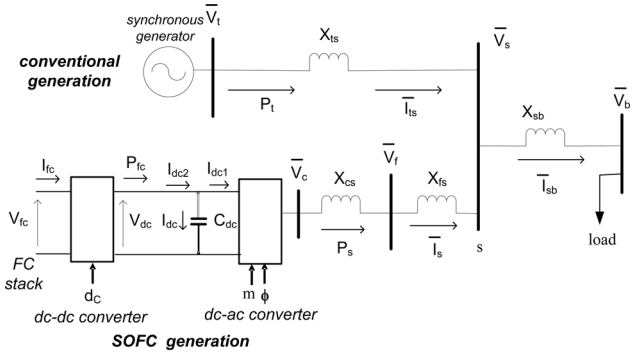

Fig. 1 *Configuration of a SOFC power plant connected to a single-machine infinite-bus power system*

with $\boldsymbol{X}_g = [\,\delta \quad \omega \quad E'_q \quad E'_{fd}\,]^{\mathrm{T}}$ and where

$$\begin{aligned}
P_t &= E'_q i_{tsq} + (x_q - x'_d) i_{tsd} i_{tsq} \\
E_q &= E'_q - (x_d - x'_d) i_{tsd} \\
V_t &= \sqrt{v_{td}^2 + v_{tq}^2} = \sqrt{(x_q i_{tsq})^2 + (E'_q - x'_d i_{tsd})^2}
\end{aligned} \tag{2}$$

Fig. 2 shows the function block diagram of the SOFC generation, dynamic model of which is given as follows [3–7]:

1. FC electrical dynamic describes the conversion of FC control to the requirement of control of FC output current, I_{fc}. That is

$$I_{\text{fc-ref}} = \frac{P_{\text{fc-ref}}}{V_{fc}} \tag{3}$$

To ensure the FC operation within the safe operating area, $I_{\text{fc-ref}}$ is limited by the following boundaries

$$\begin{aligned}
I_{\text{fc-ref-max}} &= \frac{U_{\max}}{2K_r} q_{\text{h2-in}}, \quad I_{\text{fc-ref-min}} = \frac{U_{\min}}{2K_r} q_{\text{h2-in}}, \\
K_r &= \frac{N_0}{4F}
\end{aligned} \tag{4}$$

where $U_{\max}$ and $U_{\min}$ is the maximum and minimum fuel unitisation, respectively, N_0 is the number of cells in series in the FC stack, $q_{\text{h2-in}}$ is the hydrogen input flow rate and F is the Faraday constant. Electrical dynamic describes the chemical reaction to restore the charge that has been drained by the load, which is generally fast. A first-order transfer function is used to model the dynamic with the time constant around 0.08 s.

$$I_{fc} = \frac{1}{1 + T_e s} I_{\text{fc-ref}} \tag{5}$$

2. Fuel processor depicts the dynamic of fuel supply by a first-order transfer function

$$q_{\text{h2-in}} = \frac{2K_r}{U_{\text{opt}}} \frac{1}{1 + T_f s} I_{\text{fc-ref}} \tag{6}$$

where U_{opt} is the optimal fuel utilisation and T_f is the time constant of dynamic of fuel supply.

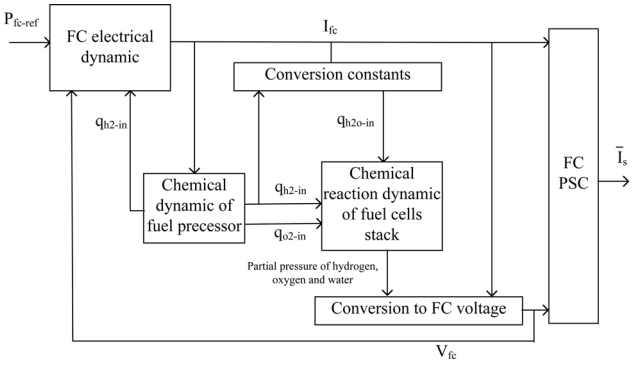

Fig. 2 *Function block diagram of a SOFC*

doi: 10.1049/iet-rpg.2010.0024

3. Blocks of 'conversion constants' and 'chemical reaction' in Fig. 2 represent the chemical process of fuel reaction inside the FC stack. Its dynamic is described by three first-order transfer functions for hydrogen, oxygen and water, respectively.

$$\begin{aligned} q_{\text{o2-in}} &= \frac{1}{r_{\text{ho}}} q_{\text{h2-in}} \\ p_{\text{h2}} &= \frac{1}{K_{\text{h2}}} \frac{1}{1+T_{\text{h2}}s}(q_{\text{h2-in}} - 2K_r I_{\text{fc}}) \\ p_{\text{o2}} &= \frac{1}{K_{\text{o2}}} \frac{1}{1+T_{\text{o2}}s}(q_{\text{o2-in}} - K_r I_{\text{fc}}) \\ p_{\text{h2o}} &= \frac{1}{K_{\text{h2o}}} \frac{1}{1+T_{\text{h2o}}s} 2K_r I_{\text{fc}} \end{aligned} \tag{7}$$

where r_{ho} is the ratio of hydrogen to oxygen, K_{h2}, K_{o2} and K_{h2o} is the valve molar constant for hydrogen, oxygen and water, T_{h2}, T_{o2} and T_{h2o} is the time constant for hydrogen, oxygen and water flow, and p_{h2}, p_{o2} and p_{h2o} the hydrogen, oxygen and water partial pressure, respectively.

4. The FC stack voltage is given by the following equation

$$V_{\text{fc}} = N_0\left[E_0 + \frac{RT}{2F}\ln\left(\frac{p_{\text{h2}} \times p_{\text{o2}}^{0.5}}{p_{\text{h2o}}}\right)\right] - rI_{\text{fc}} \tag{8}$$

where E_0 is the ideal standard potential, R is the universal gas constant, T is the absolute temperature and r is the ohmic loss.

5. Power electronics interface of the SOFC power plant with the power system consists of a dc–dc converter; a dc–ac converter (as shown in Fig. 2) and their associated controllers. FC output current control is realised by the regulation of dc–dc converter

$$d_{\text{c}} = d_{\text{c0}} + T_{\text{dc}}(s)(I_{\text{fc-ref}} - I_{\text{fc}}) \tag{9}$$

where d_{c} is the duty cycle, $T_{\text{dc}}(s)$ is the transfer function of FC current controller.

From phasor diagram of Fig. 3*a*, in the d–q coordinate of the generator, the ac voltage at the terminal of dc–ac converter can be obtained to be [11]

$$\bar{V}_{\text{c}} = mkV_{\text{dc}}(\cos\psi + j\sin\psi) = mkV_{\text{dc}}\angle\psi \tag{10}$$

where k is the converter ratio dependent on its structure (typically, $k = 3/4$ [11]), m and ϕ in Fig. 3 is the modulation ratio and phase of the pulse width modulation (PWM) control algorithm of the dc–ac converter, respectively [11]. Active power received by the grid from the SOFC power plant is

$$V_{\text{dc}}I_{\text{dc1}} = i_{sd}v_{cd} + i_{sq}v_{cq} = i_{sd}mkV_{\text{dc}}\cos\psi + i_{sq}mkV_{\text{dc}}\sin\psi$$

where i_{sd} and i_{sq} is the d and q component of $\bar{I}_{\text{s}}$, v_{cd} and v_{cq} that of $\bar{V}_{\text{c}}$, respectively. Hence

$$I_{\text{dc1}} = i_{sd}mk\cos\psi + i_{sq}mk\sin\psi \tag{11}$$

The active power supply from the SOFC power plant is $P_{\text{fc}} = I_{\text{fc}}V_{\text{fc}} = I_{\text{dc2}}V_{\text{dc}}$ and $V_{\text{dc}} = V_{\text{fc}}/(1 - d_{\text{c}})$. Hence

$$I_{\text{dc2}} = (1 - d_{\text{c}})I_{\text{fc}} \tag{12}$$

Dynamic equation of the dc–ac converter is

$$\begin{aligned} \dot{V}_{\text{dc}} &= \frac{1}{C_{\text{dc}}}I_{\text{dc}} = \frac{1}{C_{\text{dc}}}(I_{\text{dc2}} - I_{\text{dc1}}) \\ &= \frac{1}{C_{\text{dc}}}[(1 - d_{\text{c}})I_{\text{fc}} - (i_{sd}mk\cos\psi + i_{sq}mk\sin\psi)] \end{aligned} \tag{13}$$

In order to implement the PWM control algorithm to realise dc–ac conversion, the dc voltage across the capacitor, V_{dc}, should be maintained constant [5, 11]. This is the request from the PWM algorithm and it is met by applying a dc voltage controller [5, 11]. The modulation ratio is usually controlled to regulate the magnitude of the ac voltage V_{s}, that is, exchange of reactive power between the SOFC power plant and the power system. That is

$$\begin{aligned} &\text{dc voltage control: } \phi = \phi_0 + T_{\text{vdc}}(s)(V_{\text{dc}} - V_{\text{dc-ref}}) \\ &\text{ac voltage control: } m = m_0 + T_{\text{vac}}(s)(V_{\text{s}} - V_{\text{s-ref}}) \end{aligned} \tag{14}$$

where $T_{\text{vdc}}(s)$ and $T_{\text{vac}}(s)$ is the transfer function of dc and ac voltage controller, respectively.

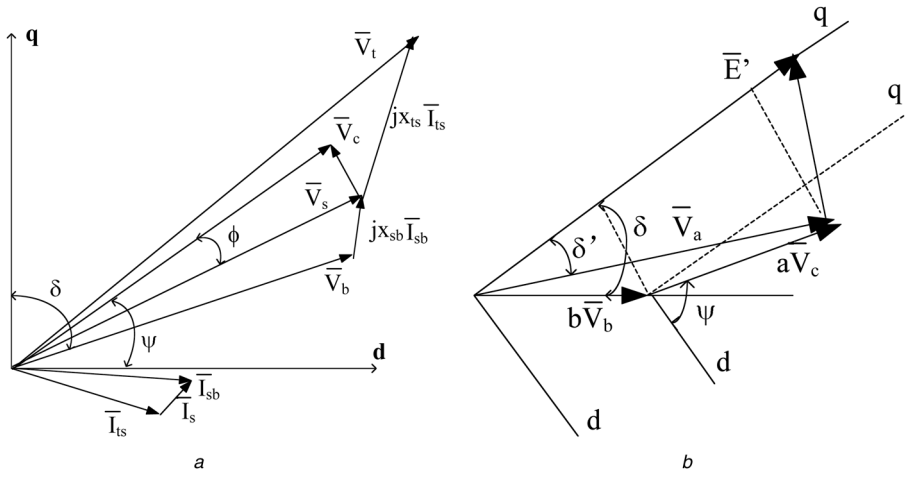

Fig. 3 *Phasor diagram of power system of Fig. 1*

From Fig. 1 it can have

$$\begin{aligned}\bar{V}_t &= jx_{ts}\bar{I}_{ts} + \bar{V}_s \\ \bar{V}_s &= -j(x_{cs} + x_{fs})\bar{I}_s + \bar{V}_c = -jx_s\bar{I}_s + \bar{V}_c \\ \bar{V}_s - \bar{V}_b &= jx_{sb}(\bar{I}_{ts} + \bar{I}_s)\end{aligned} \tag{15}$$

The above equations give

$$\begin{aligned}-jx_s\bar{I}_s + \bar{V}_c - \bar{V}_b &= jx_{sb}(\bar{I}_{ts} + \bar{I}_s) \\ \bar{V}_t &= jx_{ts}\bar{I}_{ts} + jx_{sb}(\bar{I}_{ts} + \bar{I}_s) + \bar{V}_b\end{aligned} \tag{16}$$

In d–q coordinate of the generator, as shown by Fig. 3, from (15) it can be obtained that

$$\begin{bmatrix} x_{sb} & x_s + x_{sb} \\ x_q + x_{ts} + x_{sb} & x_{sb} \end{bmatrix}\begin{bmatrix} i_{tsq} \\ i_{sq} \end{bmatrix} = \begin{bmatrix} -V_c\cos\psi + V_b\sin\delta \\ V_b\sin\delta \end{bmatrix}$$

$$\begin{bmatrix} x_{sb} & x_s + x_{sb} \\ x'_d + x_{ts} + x_{sb} & x_{sb} \end{bmatrix}\begin{bmatrix} i_{tsd} \\ i_{sd} \end{bmatrix} = \begin{bmatrix} V_c\sin\psi - V_b\cos\delta \\ E'_q - V_b\cos\delta \end{bmatrix} \tag{17}$$

The complete mathematical model of the power system of Fig. 1 is thus established, which consisted of the model of generator of (1), SOFC power plant of (3)–(9), (13) and (14), and integration of the generator and the SOFC power plant with the rest of the power system of (17).

The dynamic model of SOFC is the same as that of the low-temperature proton exchange membrane fuel cell (PEMFC), which is the most widely used type for the portable, vehicular and residential applications [12, 13]. Hence the following work should also be applicable to the PEMFC. However, for the grid-connected applications of stationary power generation, the SOFC is considered to have more significant potential, as the PEMFC is of relatively lower efficiency and depends on pure hydrogen as the fuel input [1, 2]. Hence the SOFC is used in this paper.

3 Small-signal stability analysis

3.1 Linearised model

From (10) it can have $V_c = kmV_{dc}$, that is, $\Delta V_c = k(m_0\Delta V_{dc} + V_{dc0}\Delta m)$, linearisation of (17) can be obtained to be (see equations at the bottom of the page)

The above equation can be written as

$$\begin{aligned}[\Delta i_{tsd} \quad \Delta i_{tsq}]^T &= \boldsymbol{B}_{g\text{-}fc}[\Delta\delta \quad \Delta E'_q \quad \Delta V_{dc} \quad \Delta m \quad \Delta\psi]^T \\ [\Delta i_{sd} \quad \Delta i_{sq}]^T &= \boldsymbol{B}_{fc\text{-}g}[\Delta\delta \quad \Delta E'_q \quad \Delta V_{dc} \quad \Delta m \quad \Delta\psi]^T\end{aligned} \tag{18}$$

where

$$\boldsymbol{B}_{g\text{-}fc} = \begin{bmatrix} b_{31} & b_{32} & b_{33} & b_{34} & b_{35} \\ b_{11} & b_{12} & b_{13} & b_{14} & b_{15} \end{bmatrix}$$

$$\boldsymbol{B}_{fc\text{-}g} = \begin{bmatrix} b_{41} & b_{42} & b_{43} & b_{44} & b_{45} \\ b_{21} & b_{22} & b_{23} & b_{24} & b_{25} \end{bmatrix}$$

Linearisation of (14) is

$$\begin{aligned}&\text{dc voltage control: } \Delta\phi = T_{vdc}(s)\Delta V_{dc} \\ &\text{ac voltage control: } \Delta m = T_{vac}(s)\Delta V_s\end{aligned}$$

$$\begin{bmatrix} \Delta i_{tsq} \\ \Delta i_{sq} \end{bmatrix} = \begin{bmatrix} x_{sb} & x_s + x_{sb} \\ x_q + x_{ts} + x_{sb} & x_{sb} \end{bmatrix}^{-1}\begin{bmatrix} -k\cos\psi_0(m_0\Delta V_{dc} + V_{dc0}\Delta m) + V_b\cos\delta_0\Delta\delta + V_{c0}\sin\psi_0\Delta\psi \\ V_b\cos\delta_0\Delta\delta \end{bmatrix}$$

$$= \frac{1}{x_{sb}^2 - (x_s + x_{sb})(x_q + x_{ts} + x_{sb})}\begin{bmatrix} x_{sb} & -x_s - x_{sb} \\ -x_q - x_{ts} - x_{sb} & x_{sb} \end{bmatrix}$$

$$\begin{bmatrix} V_b\cos\delta_0 & 0 & -k\cos\psi_0 m_0 & -k\cos\psi_0 V_{dc0} & V_{c0}\sin\psi_0 \\ V_b\cos\delta_0 & 0 & 0 & 0 & 0 \end{bmatrix}\begin{bmatrix} \Delta\delta \\ \Delta E'_q \\ \Delta V_{dc} \\ \Delta m \\ \Delta\psi \end{bmatrix} = \begin{bmatrix} b_{11} & b_{12} & b_{13} & b_{14} & b_{15} \\ b_{21} & b_{22} & b_{23} & b_{24} & b_{25} \end{bmatrix}\begin{bmatrix} \Delta\delta \\ \Delta E'_q \\ \Delta V_{dc} \\ \Delta m \\ \Delta\psi \end{bmatrix}$$

$$\begin{bmatrix} \Delta i_{tsd} \\ \Delta i_{sd} \end{bmatrix} = \begin{bmatrix} x_{sb} & x_s + x_{sb} \\ x'_d + x_{ts} + x_{sb} & x_{sb} \end{bmatrix}^{-1}\begin{bmatrix} k\sin\psi_0(m_0\Delta V_{dc} + V_{dc0}\Delta m) + V_{c0}\cos\psi_0\Delta\psi + V_b\sin\delta_0\Delta\delta \\ \Delta E'_q + V_b\sin\delta_0\Delta\delta \end{bmatrix}$$

$$= \frac{1}{x_{sb}^2 - (x_s + x_{sb})(x'_d + x_{ts} + x_{sb})}\begin{bmatrix} x_{sb} & -x_s - x_{sb} \\ -x'_d - x_{ts} - x_{sb} & x_{sb} \end{bmatrix}$$

$$\begin{bmatrix} V_b\sin\delta_0 & 0 & k\sin\psi_0 m_0 & k\sin\psi_0 V_{dc0} & V_{c0}\cos\psi_0 \\ V_b\sin\delta_0 & 1 & 0 & 0 & 0 \end{bmatrix}\begin{bmatrix} \Delta\delta \\ \Delta E'_q \\ \Delta V_{dc} \\ \Delta m \\ \Delta\psi \end{bmatrix} = \begin{bmatrix} b_{31} & b_{32} & b_{33} & b_{34} & b_{35} \\ b_{41} & b_{42} & b_{43} & b_{44} & b_{45} \end{bmatrix}\begin{bmatrix} \Delta\delta \\ \Delta E'_q \\ \Delta V_{dc} \\ \Delta m \\ \Delta\psi \end{bmatrix}$$

doi: 10.1049/iet-rpg.2010.0024

Since $\bar{V}_s = jx_s\bar{I}_s + \bar{V}_c$ and $V_s = \sqrt{v_{sd}^2 + v_{sq}^2}$, it can have

$$v_{sd} = -x_s i_{sq} + kmV_{dc}\cos\psi, \quad v_{sq} = x_s i_{sd} + kmV_{dc}\sin\psi$$

By using (18), linearisation of the above equations can be obtained to be (see details in Appendix 1)

$$\Delta V_s = B_1\Delta\delta + B_2\Delta E'_q + B_{dc}\Delta V_{dc} + B_3\Delta m + B_4\Delta\psi$$

Hence

$$\begin{aligned}&\text{dc voltage control: } \Delta\phi = T_{vdc}(s)\Delta V_{dc}\\ &\text{ac voltage control: } \Delta m = -T_{vac}(s)(B_1\Delta\delta + B_2\Delta E'_q\\ &\qquad + B_{dc}\Delta V_{dc} + B_3\Delta m + B_4\Delta\psi)\end{aligned} \tag{19}$$

Linearisation of mathematical expressions of the SOFC power plant of (3)–(14) is (see details in Appendix 2)

$$\dot{\boldsymbol{X}}_{fc} = \boldsymbol{A}'_{fc}\boldsymbol{X}_{fc} + \boldsymbol{B}'_{fc1}\begin{bmatrix}\Delta i_{sd} & \Delta i_{sq}\end{bmatrix}^T + \boldsymbol{B}'_{fc2}\begin{bmatrix}\Delta m & \Delta\psi\end{bmatrix}^T$$

where $\boldsymbol{X}_{fc} = \begin{bmatrix}\Delta V_{dc} & \Delta I_{fc} & \Delta q_{h2\text{-}in} & \Delta p_{h2} & \Delta p_{h2o} & \Delta p_{o2} & \boldsymbol{X}_d\end{bmatrix}^T$. By using (18), the above equation becomes

$$\begin{aligned}\dot{\boldsymbol{X}}_{fc} &= \boldsymbol{A}'_{fc}\boldsymbol{X}_{fc} + \boldsymbol{B}'_{fc1}\boldsymbol{B}_{fc\text{-}g}\begin{bmatrix}\Delta\delta & \Delta E'_q & \Delta V_{dc} & \Delta m & \Delta\psi\end{bmatrix}^T\\ &\quad + \boldsymbol{B}'_{fc2}\begin{bmatrix}\Delta m & \Delta\psi\end{bmatrix}^T\\ &= \boldsymbol{A}_{fc}\boldsymbol{X}_{fc} + \boldsymbol{B}_{fc1}\begin{bmatrix}\Delta\delta & \Delta E'_q\end{bmatrix}^T + \boldsymbol{B}_{fc2}\begin{bmatrix}\Delta m & \Delta\psi\end{bmatrix}^T\end{aligned} \tag{20}$$

By using (17), linearisation of (2) can be obtained to be

$$\begin{aligned}\Delta P_t &= K_1\Delta\delta + K_2\Delta E'_q + K_{pdc}\Delta V_{dc} + K_{pm}\Delta m + K_{p\psi}\Delta\psi\\ \Delta E_q &= K_4\Delta\delta + K_3\Delta E'_q + K_{qdc}\Delta V_{dc} + K_{qm}\Delta m + K_{q\psi}\Delta\psi\\ \Delta V_t &= K_5\Delta\delta + K_6\Delta E'_q + K_{vdc}\Delta V_{dc} + K_{vm}\Delta m + K_{v\psi}\Delta\psi\end{aligned} \tag{21}$$

where

$$\begin{aligned}K_1 &= [E'_{q0} + (x_q - x'_d)i_{tsd0}]b_{11} + (x_q - x'_d)i_{tsq0}b_{31}\\ K_2 &= [E'_{q0} + (x_q - x'_d)i_{tsd0}]b_{12} + i_{tsq0} + (x_q - x'_d)i_{tsq0}b_{32}\\ K_{pdc} &= [E'_{q0} + (x_q - x'_d)i_{tsd0}]b_{13} + (x_q - x'_d)i_{tsq0}b_{33}\\ K_{pm} &= [E'_{q0} + (x_q - x'_d)i_{tsd0}]b_{14} + (x_q - x'_d)i_{tsq0}b_{34}\\ K_{p\psi} &= [E'_{q0} + (x_q - x'_d)i_{tsd0}]b_{15} + (x_q - x'_d)i_{tsq0}b_{35}\\ K_3 &= 1 - (x_d - x'_d)b_{32}, \quad K_4 = -(x_d - x'_d)b_{31}\\ K_{qdc} &= -(x_d - x'_d)b_{33}\\ K_{qm} &= -(x_d - x'_d)b_{34}, \quad K_{q\psi} = -(x_d - x'_d)b_{35}\\ K_5 &= \frac{v_{td0}}{V_{t0}}x_q b_{11} - \frac{v_{tq0}}{V_{t0}}x'_d b_{31}\\ K_6 &= \frac{v_{td0}}{V_{t0}}x_q b_{12} + \frac{v_{tq0}}{V_{t0}}(1 - x'_d b_{32})\\ K_{vdc} &= \frac{v_{td0}}{V_{t0}}x_q b_{13} - \frac{v_{tq0}}{V_{t0}}x'_d b_{33}, \quad K_{vm} = \frac{v_{td0}}{V_{t0}}x_q b_{14} - \frac{v_{tq0}}{V_{t0}}x'_d b_{34}\\ K_{v\psi} &= \frac{v_{td0}}{V_{t0}}x_q b_{15} - \frac{v_{tq0}}{V_{t0}}x'_d b_{35}\end{aligned}$$

Thus linearisation of dynamic model of the generator of (1) can be obtained to be

$$\begin{aligned}\Delta\dot{\delta} &= \omega_o\Delta\omega\\ \Delta\dot{\omega} &= \frac{1}{M}(-K_1\Delta\delta - D\Delta\omega - K_2\Delta E'_q - K_{pdc}\Delta V_{dc}\\ &\quad - K_{pm}\Delta m - K_{p\psi}\Delta\psi)\\ \Delta\dot{E}'_q &= \frac{1}{T'_{d0}}(-K_4\Delta\delta - K_3\Delta E'_q + \Delta E'_{fd} - K_{qdc}\Delta V_{dc}\\ &\quad - K_{qm}\Delta m - K_{q\psi}\Delta\psi)\\ \Delta\dot{E}'_{fd} &= -\frac{1}{T_A}\Delta E'_{fd} - \frac{K_A}{T_A}(\Delta\delta + K_6\Delta E'_q + K_{vdc}\Delta V_{dc}\\ &\quad + K_{vm}\Delta m + K_{v\psi}\Delta\psi)\end{aligned} \tag{22}$$

Equations (19), (20) and (22) form the complete linearised model of the power system integrated with the SOFC power plant, which can be shown by Fig. 4. In Fig. 4, the block of ac and dc voltage control function is given by (19). This linearised model of Fig. 4 is quite similar to the conventional Phillips–Heffron model [8, 14, 15] based on which the technique of damping torque analysis was developed for the study of power system small-signal stability. In Fig. 4, ΔT_{ET} is the electric torque contribution, which can be decomposed into the synchronising torque

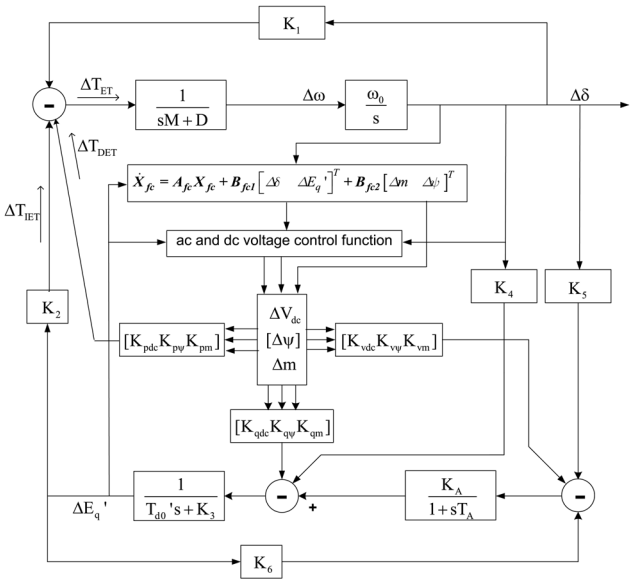

Fig. 4 *Linearised model of the power system integrated with the SOFC power plant of Fig. 1*

and the damping torque. The damping torque component decides the damping of power system oscillation [8, 15].

According to the principle of superimposition of linear systems, the forward path from the SOFC power plant to the electromechanical oscillation loop of the synchronous generator is obtained by setting $K_1 = K_4 = K_5 = 0$ [8–10, 15, 16]. Thus electric torque $\Delta T_{\rm ET}$ is contributed purely from the SOFC power plant and its associated control functions. $\Delta T_{\rm ET}$ can be divided into the direct electric torque contribution, $\Delta T_{\rm DET}$, and the indirect electric torque contribution, $\Delta T_{\rm IET}$, as shown in Fig. 4. Usually, the direct electric torque is much greater than the indirect electric torque [16]. From Fig. 4 it can be seen that obviously, the coefficient, $K_{p\rm dc}$, $K_{p\psi}$ and K_{pm} mostly affect the amount of electric torque contribution from the SOFC power plant and its associated control functions and

$$K_{p\rm dc} = \frac{\partial P_t}{\partial V_{\rm dc}}, \quad K_{p\psi} = \frac{\partial P_t}{\partial \psi}, \quad K_{pm} = \frac{\partial P_t}{\partial m} \tag{23}$$

3.2 Explicit expression of active power delivered along the transmission line

From (15) it can have

$$\bar{I}_s = \frac{\bar{V}_c - \bar{V}_s}{jx_s}$$

Thus

$$\bar{V}_{\rm s} - \bar{V}_{\rm b} = jx_{\rm sb}\bar{I}_{\rm ts} + \frac{x_{\rm sb}}{x_{\rm s}}\bar{V}_{\rm c} - \frac{x_{\rm sb}}{x_{\rm s}}\bar{V}_{\rm s}$$

The above equation gives

$$\bar{V}_S = \frac{jx_{\rm sb}}{1 + (x_{\rm sb}/x_S)}\bar{I}_{\rm ts} + \frac{x_{\rm sb}}{x_S(1 + (x_{\rm sb}/x_S))}\bar{V}_C + \frac{\bar{V}_{\rm b}}{1 + (x_{\rm sb}/x_S)} \tag{24}$$

That gives

$$\bar{V}_{\rm t} = jx_{\rm ts}\bar{I}_{\rm ts} + \bar{V}_S = j\left(x_{\rm ts} + \frac{x_S x_{\rm sb}}{x_S + x_{\rm sb}}\right)\bar{I}_{\rm ts} + \frac{x_{\rm sb}}{x_S + x_{\rm sb}}\bar{V}_C + \frac{x_S}{x_S + x_{\rm sb}}\bar{V}_{\rm b} = jx\bar{I}_{\rm ts} + \bar{V}_a \tag{25}$$

where

$$x = \left(x_{\rm ts} + \frac{x_S x_{\rm sb}}{x_S + x_{\rm sb}}\right)$$

$$\bar{V}_a = \frac{x_{\rm sb}}{x_S + x_{\rm sb}}\bar{V}_C + \frac{x_S}{x_S + x_{\rm sb}}\bar{V}_{\rm b} = a\bar{V}_C + b\bar{V}_{\rm b}$$

For a single-machine infinite-bus power system WITHOUT the SOFC power plant, the terminal voltage equation of the generator is

$$\bar{V}_{\rm t} = jx_{\rm t}\bar{I}_{\rm t} + \bar{V} \tag{26}$$

where $x_{\rm t}$ is the equivalent reactance of the transmission line, $\bar{I}_{\rm t}$ is the line current and $\bar{V}$ is the voltage at the infinite busbar. The explicit mathematical description of the active power supplied by the generator is

$$P_{\rm t} = \frac{E'_q V}{x'_{d\Sigma}}\sin\delta - \frac{V^2}{2}\frac{(x_q - x'_d)}{x'_{d\Sigma}x_{q\Sigma}}\sin 2\delta \tag{27}$$

where δ is the angle (load angle) between E'_q (q-axis of the generator) and $\bar{V}$ and $x'_{d\Sigma} = x_{\rm t} + x'_d$, $x_{q\Sigma} = x_{\rm t} + x_q$.

Comparing (25) and (26) it can be seen that the power system integrated with the SOFC power plant of Fig. 1 is electrically equivalent to a power system without the SOFC power plant with an equivalent line reactance to be x and voltage at the 'infinite busbar' to be $\bar{V}_a$. Hence by replacing $x_{\rm t}$ and V in (27) by x and $\bar{V}_a$, respectively, the explicit mathematical description of the active power supplied by the generator in the power system of Fig. 1 can be obtained to be

$$P_{\rm t} = \frac{E'_q V_a}{x'_{d\Sigma}}\sin\delta' - \frac{V_a^2}{2}\frac{(x_q - x'_d)}{x'_{d\Sigma}x_{q\Sigma}}\sin 2\delta' \tag{28}$$

where δ' is the angle between E'_q and $\bar{V}_a$ and $x'_{d\Sigma} = x + x'_d$, $x_{q\Sigma} = x + x_q$. Normally, in (28) the first part is much greater than the second part [6]. Hence it can have

$$P_{\rm t} \simeq \frac{E'_q V_a}{x'_{d\Sigma}}\sin\delta' \tag{29}$$

From the phasor diagram of Fig. 3*b* it can have $V_a \sin\delta' = bV_b \sin\delta + aV_c \cos\psi$, from which and (29) it can have

$$P_{\rm t} \simeq \frac{E'_q}{x'_{d\Sigma}}(bV_b \sin\delta + aV_c \cos\psi) \tag{30}$$

where $V_c = mkV_{\rm dc}$.

Hence from (23) and (30) it can have

$$K_{p\rm dc} = \frac{E'_{q0}}{x'_{d\Sigma}}am_0\, k\cos\psi_0$$

$$K_{p\psi} = -\frac{E'_{q0}}{x'_{d\Sigma}}am_0\, kV_{\rm dc0}\sin\psi_0 \tag{31}$$

$$K_{pm} = \frac{E'_{q0}}{x'_{d\Sigma}}akV_{\rm dc0}\cos\psi_0$$

3.3 Damping torque analysis

From Appendix 1 it has

$$\Delta\psi = g\Delta\phi + g_1\Delta\delta + g_2\Delta E'_q + g_{\rm dc}\Delta V_{\rm dc} + g_3\Delta m \tag{32}$$

When only the electric torque through the ac voltage control is considered ($\Delta\phi = 0$ hence $\Delta V_{\rm dc} = 0$), from (19) and (32) it can have

$$\Delta m = -T_{\rm vac}(s)[(B_1 + B_4 g_1)\Delta\delta + (B_2 + B_4 g_2)\Delta E'_q + (B_3 + B_4 g_3)\Delta m]$$

doi: 10.1049/iet-rpg.2010.0024

Thus

$$\Delta m = \frac{T_{\text{vac}}(s)}{1-(B_3+B_4 g_3)T_{\text{vac}}(s)}[(B_1+B_4 g_1)\Delta\delta + (B_2+B_4 g_2)\Delta E'_q] \quad (33)$$

The direct electric torque contribution from the SOFC generation through the ac voltage controller (the indirect electric torque is ignored, that is equivalent to that $\Delta E'_q \simeq 0$ in the computation of electric torque) can be obtained from (31), (33) and Fig. 4 to be

$$\Delta T_{\text{DET}} = \frac{E'_{q0}}{x'_{d\Sigma}} akV_{\text{dc0}} \cos\psi_0 \frac{T_{\text{vac}}(s)}{1-(B_3+B_4 g_3)T_{\text{vac}}(s)} \times (B_1+B_4 g_1)\Delta\delta \quad (34)$$

Based on (34), effect of the FC AC voltage control on power system small-signal stability can be examined. For example, if it is a proportional controller with $T_{\text{vac}}(s) = K_{\text{vac}}$, (34) becomes

$$\Delta T_{\text{DET}} = \frac{E'_{q0}}{x'_{d\Sigma}} akV_{\text{dc0}} \cos\psi_0 \frac{K_{\text{vac}}}{1-(B_3+B_4 g_3)K_{\text{vac}}} \times (B_1+B_4 g_1)\Delta\delta \quad (35)$$

The electric torque is mainly the synchronising torque and hence the ac voltage control is of very small influence on the damping of power system oscillations. Same conclusion has been established for other types of power system devices [15, 16] by using the similar analysis.

When only the direct electric torque (equivalent to set $\Delta E'_q \simeq 0$) from the SOFC power plant through the dc voltage control is considered ($\Delta m = 0$), from (19), (31), (32) and Fig. 4, it can have

$$\begin{aligned}\Delta T_{\text{DET}} &= \frac{E'_{q0}}{x'_{d\Sigma}} am_0 k(\cos\psi_0\Delta V_{\text{dc}} - V_{\text{dc0}}\sin\psi_0\Delta\psi)\\ &= -\frac{E'_{q0}}{x'_{\text{d}\Sigma}} am_0 kV_{\text{dc0}}\sin\psi_0 g_1\Delta\delta\\ &\quad + \frac{E'_{q0}}{x'_{\text{d}\Sigma}} am_0 k(\cos\psi_0\Delta V_{\text{dc}} - V_{\text{dc0}}\sin\psi_0 g_{\text{dc}}\Delta V_{\text{dc}}\\ &\quad - V_{\text{dc0}}\sin\psi_0 g\Delta\phi)\\ &= -\frac{E'_{q0}}{x'_{\text{d}\Sigma}} am_0 kV_{\text{dc0}}\sin\psi_0 g_1\Delta\delta\\ &\quad + \frac{E'_{q0}}{x'_{\text{d}\Sigma}} am_0 k[\cos\psi_0 - V_{\text{dc0}}\sin\psi_0 g_{\text{dc}}V_{\text{dc0}}\\ &\quad - \sin\psi_0 gT_{\text{vdc}}(s)]\Delta V_{\text{dc}}\end{aligned} \quad (36)$$

According to the damping torque analysis given in Appendix 3, at the angular oscillation frequency, ω_s, ΔV_{dc} is approximately in the same phase with $\Delta\omega$ in small-signal power oscillations, that is, $\Delta V_{\text{dc}} \simeq C_D\Delta\omega$. Hence the damping torque (component in ΔT_{DET} which is proportional to $\Delta\omega$) provided by the SOFC power plant can be obtained to be

$$\text{Damping torque: } \Delta T_{\text{DDET}} \simeq \frac{E'_{q0}}{x'_{\text{d}\Sigma}} am_0 kC_D \times (\cos\psi_0 - V_{\text{dc0}}\sin\psi_0 g_{\text{dc}}V_{\text{dc0}} - RV_{\text{dc0}}g\sin\psi_0)C_D\Delta\omega \quad (37)$$

where R is the real part of $T_{\text{vdc}}(j\omega_s)$. In deriving the above equation, the first equation in (22) in the frequency domain, $\Delta\delta = -j(\omega_0/\omega_s)\Delta\omega$, is used.

Obviously, in $T_{\text{vdc}}(j\omega_s)$, R is proportional to the gain of the dc voltage controller. If $V_{\text{dc}} < V_{\text{dcref}}$ ($\Delta V_{\text{dc}} < 0$), the dc voltage control should enable the dc capacitor of dc–ac converter to absorb more active power from the power system to charge the capacitor. From Fig. 3 it can be seen that ψ should decrease such that $\psi < \psi_0$ ($\Delta\psi < 0$ and $\Delta\phi < 0$) to enable the injection of active power into the dc–ac converter from the power system. On the other hand, if $V_{\text{dc}} > V_{\text{dcref}}$ ($\Delta V_{\text{dc}} > 0$), ψ should increase such that $\psi > \psi_0$ ($\Delta\psi > 0$ and $\Delta\phi > 0$) to enable the injection of active power into the power system from the dc–ac converter. Hence, design of dc voltage controller must have $R > 0$. Similarly and according to (32), g should also be positive. On the other hand, from Fig. 3 it can be seen that ψ_0 changes with the variations of power system load conditions. Since $V_{\text{dc0}} > 0$, (37) indicates that the damping torque contribution from the SOFC power plant varies with changes of load conditions of the power systems. Especially it changes sign when $(\cos\psi_0 - V_{\text{dc0}}\sin\psi_0 g_{\text{dc}}V_{\text{dc0}} - RV_{\text{dc0}}g\sin\psi_0) = 0$, which gives

$$\psi_{0\text{-critical}} \simeq \tan^{-1}\left(\frac{1}{V_{\text{dc0}}g_{\text{dc}}V_{\text{dc0}} + RgV_{\text{dc0}}}\right) \quad (38)$$

$\psi_{0\text{-critical}}$ in the above equation defines a critical angle as far as the effect of the SOFC power plant on the small-signal stability of the power system is concerned. When the SOFC power plant operates beyond the critical angle, the SOFC power plant provides negative damping torque and hence affects power system small-signal stability negatively. Similar to the concept of steady-state stability limit in the single-machine infinite-bus power system which is defined to be the maximum load angle $\delta_{\max}$ in the phasor diagram of Fig. 3 (normally $\delta_{\max} = 90^\circ$ [8]), the critical angle, $\psi_{0\text{-critical}}$, can be defined as the stability limit of operation of the SOFC power plant, as far as the small-signal stability of power system is considered. In Appendix 4, an algorithm is demonstrated to compute the accurate value of $\psi_{0\text{-critical}}$.

4 Example of single-machine infinite-bus power system

Parameters and initial operating conditions of an example single-machine infinite-bus power system integrated with a SOFC power plant of Fig. 1 are given in Appendix 5. Computational results of damping torque contribution from the SOFC power plant, confirmed by the computational results of system oscillation mode, from the complete linearised model of (19), (20) and (22) are given in Tables 1 and 2. In Table 1, the total active power supplied by the generator and SOFC power plant to the load at the infinite busbar is fixed at 1 p.u., but the level of

Table 1 Computational results of the example power system when total active power received at the infinite busbar is fixed at 1.0 p.u. ($P_{t0} + P_{fc0} = 1.0$ p.u.)

P_{t0}, p.u.	P_{fc0}, p.u.	ψ_0 (degree)	ΔT_{Ddc}	ΔT_{Dddc}	ΔT_{Ddco}	Electromechanical oscillation mode
1.0	0.0	48.9	5.37	5.38	5.37	$-0.5729 \pm j3.8590$
0.9	0.1	54.1	3.31	3.29	3.31	$-0.4271 \pm j3.9725$
0.8	0.2	59.5	1.60	1.57	1.60	$-0.3121 \pm j4.0866$
0.7	0.3	65.1	0.19	0.15	0.20	$-0.2208 \pm j4.4944$
0.6	0.4	70.7	−0.99	−1.03	−0.98	$-0.1472 \pm j4.2940$
0.5	0.5	76.4	−1.99	−2.03	−1.99	$-0.087 \pm j4.3856$
0.4	0.6	82.3	−2.85	−2.87	−2.84	$-0.0371 \pm j4.4701$
0.3	0.7	88.2	−3.58	−3.60	−3.57	$0.0045 \pm j4.5491$
0.2	0.8	94.1	−4.22	−4.24	−4.22	$0.0393 \pm j4.6240$
0.1	0.9	100.1	−4.79	−4.80	−4.79	$0.0684 \pm j4.6960$

Table 2 Computational results of the example power system when the SOFC power generation is fixed at 0.3 p.u. ($P_{fc0} = 0.3$ p.u.)

P_{t0}, p.u.	ψ_0 (degree)	ΔT_{Ddc}	ΔT_{Dddc}	ΔT_{Ddco}	Electromechanical oscillation mode
0.1	90.7	−3.4	−3.4	−3.4	$-0.0348 \pm j4.7497$
0.2	86.3	−2.9	−2.9	−2.9	$-0.0645 \pm j4.6975$
0.3	81.9	−2.4	−2.4	−2.4	$-0.0940 \pm j4.6330$
0.4	77.6	−1.8	−1.9	−1.8	$-0.1239 \pm j4.5539$
0.5	73.3	−1.3	−1.3	−1.3	$-0.1546 \pm j4.4572$
0.6	69.1	−0.6	−-0.7	−0.6	$-0.1866 \pm j4.3391$
0.7	65.1	0.2	0.2	0.2	$-0.2208 \pm j4.1944$
0.8	61.1	1.1	1.2	1.1	$-0.2584 \pm j4.0165$
0.9	57.2	2.3	2.5	2.3	$-0.3012 \pm j3.7950$
1.0	53.4	3.8	4.1	3.8	$-0.3518 \pm j3.5119$

mixture of conventional and SOFC power generation varies. In Table 2, the SOFC power generation is fixed to be 0.3 p.u., but the active power supply from the generator changes. In Tables 1 and 2, P_{t0} and P_{fc0} is the active power supplied by the conventional generator and the FC power generation unit, respectively, ΔT_{Ddc} and ΔT_{Dddc} the total and direct damping torque provided by the FC power generation unit, respectively, and ΔT_{Ddco} is the total damping torque provided by the FC power generation unit with its AC voltage control function being switched off. From Tables 1 and 2, it can be seen that

1. The direct damping torque contribution, ΔT_{Dddc}, from the SOFC power plant is approximately equal to its total damping torque contribution ΔT_{Ddc}, as indicated in the analysis of above section, suggesting that it is appropriate to ignore the indirect damping torque.
2. The damping torque contribution from the SOFC power plant changes very little when its AC voltage control function is switched on or off ($\Delta T_{Ddc} \simeq \Delta T_{Ddco}$). This confirms the previous analysis that the AC voltage control function of the SOFC power plant affects the power system small-signal stability very little.
3. Damping torque supplied by the SOFC power plant changes at different levels of mixture of conventional and FC power generation, which can be positive or negative (Table 1), thus improving or reducing power system small-signal stability as concluded in the above section.
4. Damping torque supplied by the SOFC power plant also changes from positive to negative at different levels of conventional power generation even though the FC power generation is fixed (Table 2), thus helping or damaging the damping of power system small-signal oscillation.
5. Estimation from (38) is $\psi_{0\text{-critical}} \simeq 73^\circ$ for the example power system. A more accurate calculation gives $\psi_{0\text{-critical}} = 65.2704^\circ$ (see Appendix 4). This is confirmed by the results in Tables 1 and 2, as damping torque contribution from the SOFC power plant changes sign between $\psi_0 = 65.1^\circ$ and $\psi_0 = 70.7^\circ$ (Table 1) or $\psi_0 = 69.1^\circ$ (Table 2). Hence operation of the SOFC power plant should avoid $\psi_0 > \psi_{0\text{-critical}}$ when it provides negative damping to the power system oscillation.

In order to demonstrate the correctness of the above analysis and the computational results obtained from the linearised model of the power system, non-linear simulation of the example power system was carried out by using the full non-linear model of the power system integrated with the SOFC power plant described by (1)–(9), (13), (14) and (17). It simulated the response of the example power system when a small increase of 1% mechanical power input to the conventional power generation occurred at 1 s of simulation for 100 ms. Fig. 5 gives the results of simulation at two different levels of mixture of conventional and SOFC power generation when the total power received by the load at the infinite busbar was fixed at 1 p.u. Fig. 6 shows the results of simulation at two different levels of conventional generation and the SOFC power generation was fixed at 0.3 p.u. These results of non-linear simulation confirm both the analysis in the above section and the computational results presented in Tables 1 and 2.

1. When the total power received by the load is fixed (Fig. 6), by comparing the system response (i) in Fig. 5*a* ($P_{fc0} = 0.1$ p.u.) and the response (i) in Fig. 5*b* ($P_{fc0} = 0.9$ p.u.), it can be seen that the heavier the load

doi: 10.1049/iet-rpg.2010.0024

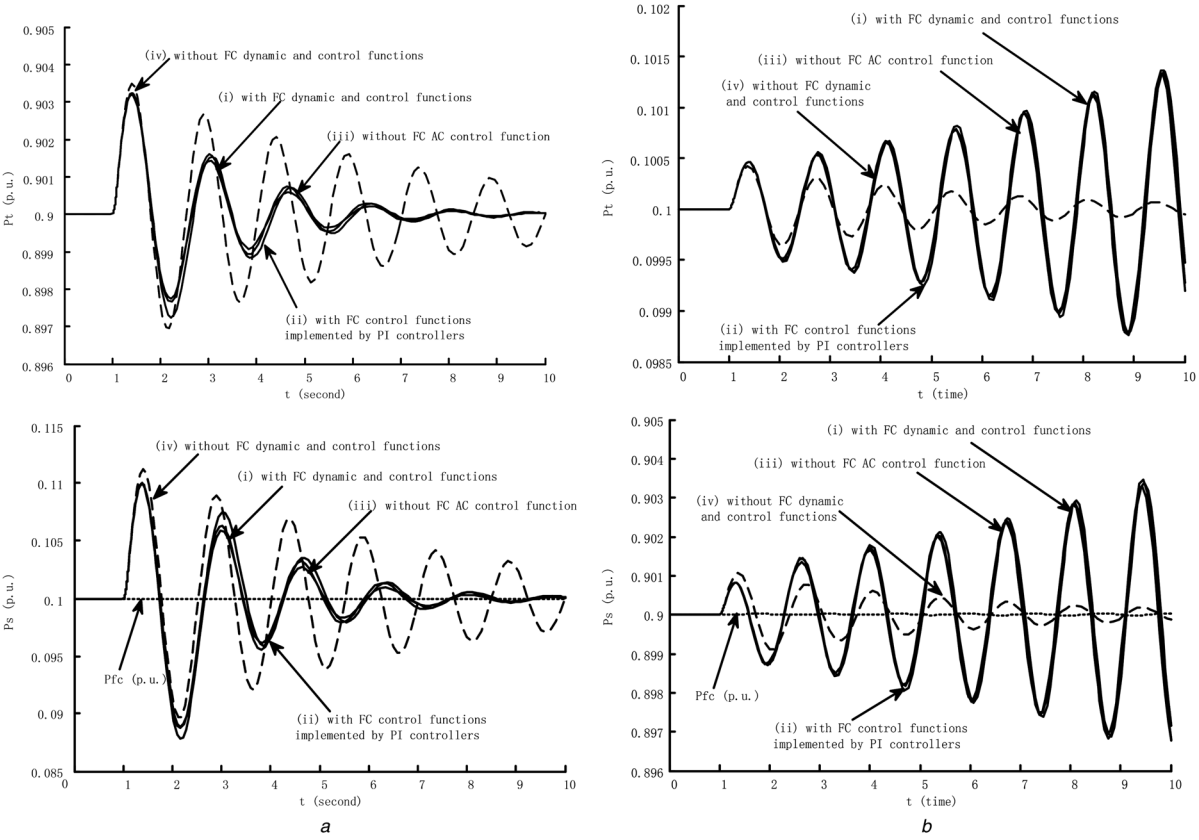

Fig. 5 *Simulation at two different levels of mixture of conventional and SOFC power generation when the total power received by the load at the infinite busbar was fixed at 1.0 p.u.*

a $P_{t0} = 0.9$ p.u. and $P_{fc0} = 0.1$ p.u.
b $P_{t0} = 0.1$ p.u. and $P_{fc0} = 0.9$ p.u.

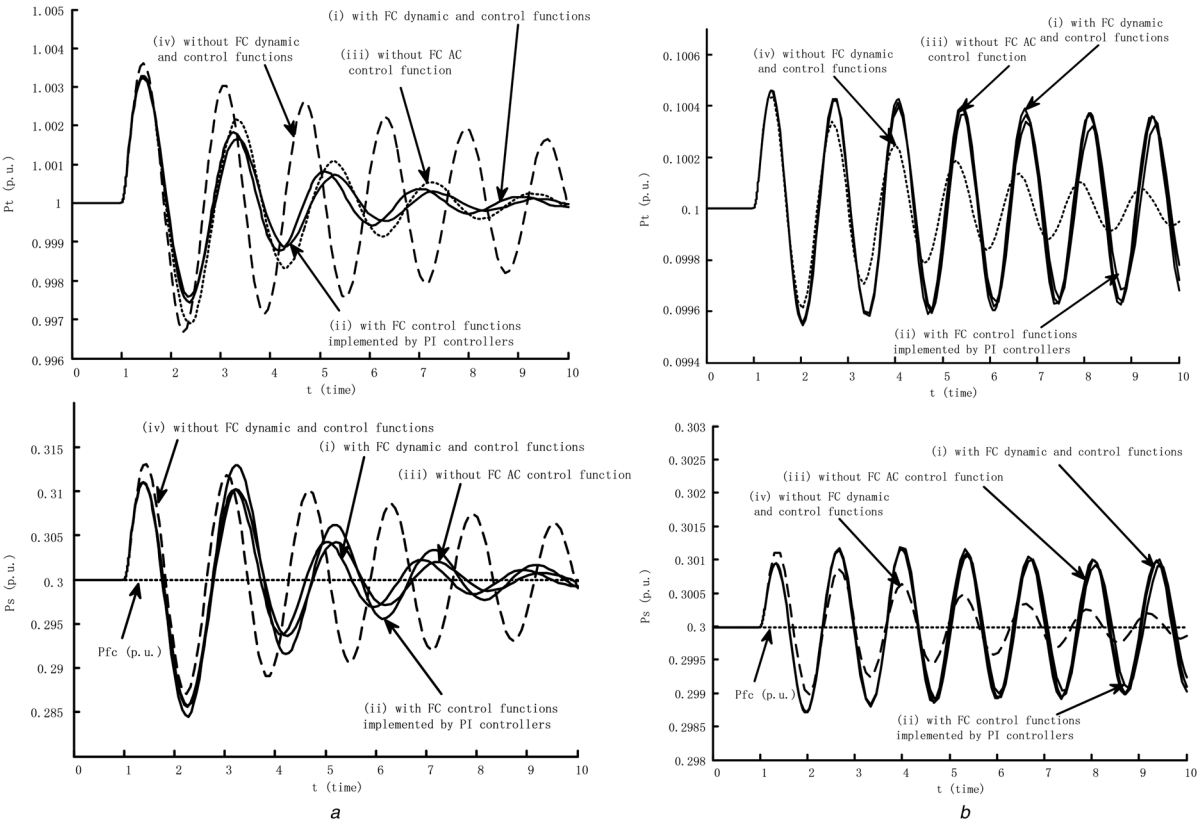

Fig. 6 *Simulation when the generator operated at two loading conditions and the SOFC power generation was fixed at 0.3 p.u.*

a $P_{t0} = 1.0$ p.u. and $P_{fc0} = 0.3$ p.u.
b $P_{t0} = 0.1$ p.u. and $P_{fc0} = 0.3$ p.u.

condition of the SOFC power plant operates at, the more it will damage the damping of power system oscillation;
2. When the SOFC power generation is fixed (Fig. 6), by comparing the system response (i) in Fig. 6*a* ($P_{t0} = 1.0$ p.u.) and the response (i) in Fig. 6*b* ($P_{t0} = 0.1$ p.u.) it can be seen that the lighter the load condition of the conventional power plant is, the more negative damping torque is provided by the SOFC power plant.
3. In Figs. 5 and 6, system response (see (ii) in Figs. 5 and 6) when the AC and DC voltage control functions of SOFC power plant are implemented by proportional integral (PI) controllers is presented. From these results it can be seen that same observations to cases (1) and (2) above are obtained.
4. In Figs. 5 and 6, system response (see (iii) in Figs. 5 and 6) with the AC voltage control function of the SOFC power plant being switched off is given. It shows that indeed it imposes very little influence on power system small-signal stability.
5. In order to demonstrate that the small-signal stability of the example power system is truly attributed to the dynamic and control functions of the SOFC power plant rather than simply because of the injection of active power from the SOFC power plant midway between the conventional generator and the large power system at the infinite busbar, in Figs. 5 and 6, system response (see (iv) in Figs. 5 and 6) when the dynamic and control functions of the SOFC power plant are switched off. This switching off is achieved by setting the DC voltage across the capacitor to be a constant (equivalent to installing a capacitor with very large capacitance) and with open-loop ac and dc voltage controllers. In this case, the SOFC power plant is connected to the system purely as an active power source. From those results (response (iv) in Figs. 5 and 6) it can be seen that without the influence of the dynamic and control functions of the SOFC power plant, the damping of power oscillation changes significantly less when the loading conditions vary. These results confirm that it is truly the dynamic and control functions of the SOFC power plant that affects the power system small-signal stability.

5 Example of multi-machine power system

Fig. 7 shows the configuration of a four-machine two-area power system integrated with a SOFC power plant. This is the modified example power system used in several occasions for the study of power system small-signal stability in [17–20] (without the SOFC power plant). Parameters of the example power system are given in [20] and Appendix 5. The SOFC adopts a current control scheme (the SOFC in the previous example uses a voltage control scheme, see Appendix 5). Power supply is through the tie line from G1, G2 and the SOFC power plant to the main load L_5 in the system. Table 3 gives the computational results of system inter-area oscillation mode [17–20] when the mixture of conventional generation from G1 and G2 and the SOFC power plant changes (other eigenvalues of the system are not listed in Table 3). From Table 3 it can be seen that with the variation of the generation mixture, the damping of system inter-area oscillation mode changes, indicating the variation of system small-signal stability. This is exactly the same to the results given in Table 1.

Fig. 8 gives the results of system simulation when the mixture of generation from G1, G2 and the SOFC changes. At 0.2 s of the simulation, the mechanical power input to G4 increased by 10% and the returned to the original value at 0.3 s of the simulation. From Fig. 8*a* it can be seen that the damping of power oscillation varies when the SOFC generation changes, although the total amount of power delivered from G1, G2 and the SOFC power plant to L_5 (i.e. P_{65}) keeps unchanged to be 2 p.u. In fact, damping of power oscillation of P_{26} is also different at the different level of mixture of conventional and the SOFC generation (see Fig. 8*b*). Hence Fig. 8 confirms the results presented in Table 3 that the small-signal stability of the example four-machine two-area power system is affected by the variation of the loading conditions of the grid-connected SOFC power plant.

Table 3 Computational results of system inter-area oscillation mode when the mixture of generation from G1, G2 and SOFC changes (P_B is fixed at 2.0 p.u.)

Mixture of generation from G1, G2 and the SOFC	System inter-area oscillation mode
$P_{26} = 1.9$ p.u., $P_{SOFC} = 0.1$ p.u.	$-0.0112 \pm j3.473$
$P_{26} = 1.45$ p.u., $P_{SOFC} = 0.55$ p.u.	$-0.0600 \pm j3.426$
$P_{26} = 1.0$ p.u., $P_{SOFC} = 1.0$ p.u.	$-0.1043 \pm j3.369$

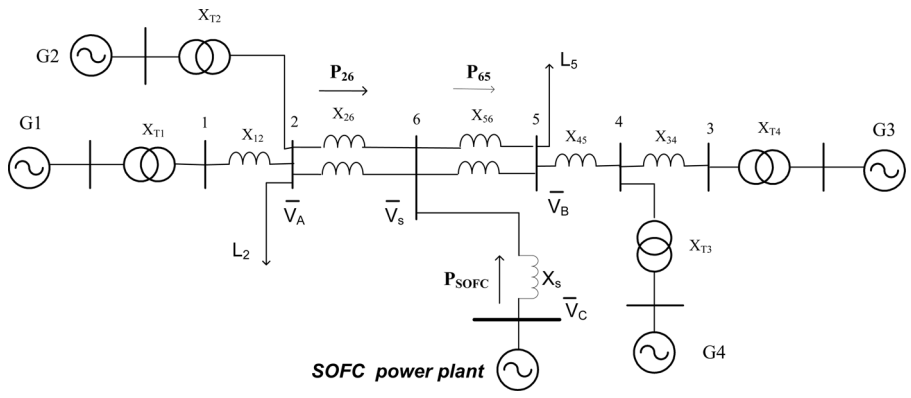

Fig. 7 *Example of multi-machine power system integrated with a SOFC generation plant*

doi: 10.1049/iet-rpg.2010.0024

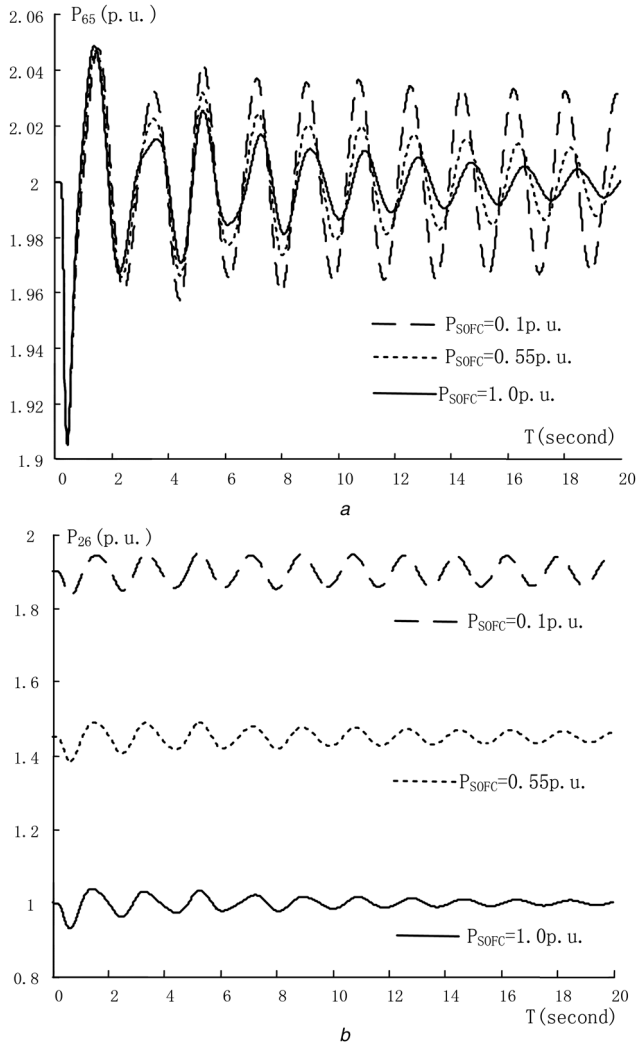

Fig. 8 *Simulation results of an example four-machine power system with the grid-connected SOFC power plant*

a Power oscillation at P_{65}
b Power oscillation at P_{26}

6 Conclusions

This paper investigates the effect of the grid-connected SOFC generation on power system small-signal stability by using the conventional technique of damping torque analysis. It is concluded in this paper that power system small-signal stability can be affected by the gird-connected SOFC generation either positively or negatively depending upon the power system's operating conditions. It is revealed in this paper that a stability limit of the operation of the SOFC power plant integrated in a single-machine infinite-bus power system, as far as system small-signal stability is concerned. The SOFC power plant should operate below the stability limit to avoid its negative effect. Results of numerical calculation and non-linear simulation of an example power system are given, which confirm the analysis presented and conclusion obtained in this paper.

In order to explore the generality of the conclusions obtained in the paper from the simple case of a single-machine infinite-bus power system integrated with a SOFC power plant, an example multi-machine power system with a grid-connected SOFC power plant is presented. The SOFC in the example of multi-machine power system employs a different type of control scheme, current control, for the network integration to that (the voltage type of control) adopted in the study of the single-machine infinite-bus power system. Results of modal computation and simulation confirm that the SOFC operating conditions affect the system small-signal stability.

7 Acknowledgments

The authors would like to acknowledge the support of the EPSRC UK–China joint research consortium (EP/F061242/1), the science bridge award (EP/G042594/1), UK, Jiangsu Power Company, China, and the Fund of Best Post-Graduate Students of Southeast University, China. Professor Haifeng Wang is a member of the international innovation team of superconducting technology for electrical engineering at the Institute of Electrical Engineering, Beijing, China, sponsored by the Chinese Academy of Sciences, China.

8 References

1 Thounthong, P., Davat, B., Rael, S., Sethakul, P.: 'Fuel cell high-power applications', *IEEE Ind. Electron. Mag.*, 2009, **3**, (1), pp. 33–46
2 Li, Y.H., Rajakaruna, S., Choi, S.S.: 'Control of a solid oxide fuel cell power plant in a grid-connected system', *IEEE Trans. Energy Convers.*, 2007, **22**, (2), pp. 405–413
3 Padulles, J., Ault, G.W., McDonald, J.R.: 'An integrated SOFC plant dynamic model for power systems simulation', *J. Power Sources*, 2000, **86**, pp. 495–500
4 Zhu, Y., Tomsovic, K.: 'Development of models for analyzing the load-following performance of microturbines and fuel cells', *Electr. Power Syst. Res.*, 2002, **62**, pp. 1–11
5 Georgakis, D., Papathanassiou, S., Manias, S.: 'Modelling and control of a small scale grid-connected PEM fuel cell system'. Proc. IEEE 36th Power Electronics Specialists Conf., 2005, pp. 1614–1620
6 Sedghisigarchi, K., Feliachi, A.: 'Dynamic and transient analysis of power distribution systems with fuel cells – part I fuel-cell dynamic model', *IEEE Trans. Energy Convers.*, 2004, **19**, (2), pp. 423–428
7 Sedghisigarchi, K., Feliachi, A.: 'Dynamic and transient analysis of power distribution systems with fuel cells – part II control and stability enhancement', *IEEE Trans. Energy Convers.*, 2004, **19**, (2), pp. 429–434
8 Yu, Y.N.: 'Electric power system dynamics' (Academic Press Inc., 1983)
9 deMello, F.P., Concordia, C.: 'Concepts of synchronous machine stability as affected by excitation control', *IEEE Trans. Power Appar. Syst.*, 1969, **88**, (4), pp. 316–329
10 Larsen, E.V., Swann, D.A.: 'Applying power system stabilizers Part I–III', *IEEE Trans. Power Appar. Syst.*, 1981, **100**, (6), pp. 3017–3046
11 'Modeling of power electronics equipment (FACTS) in load flow and stability programs', CIGRE T F 38-01-08, 1998 Q3
12 Uzunoglu, M., Alam, M.S.: 'Dynamic modeling, design, and simulation of a combined PEM fuel cell and ultracapacitor system for stand-alone residential applications', *IEEE Trans. Energy Convers.*, 2006, **21**, (3), pp. 767–775
13 Tanrioven, M., Alam, M.S.: 'Modeling, control, and power quality evaluation of a PEM fuel cell-based power supply system for residential use', *IEEE Trans. Ind. Appl.*, 2006, **42**, (6), pp. 1582–1589
14 Heffron, W.G., Phillips, R.A.: 'Effect of a modem amplidyne voltage regulator on under excited operation of large turbine generator', *AIEE Trans.*, 1952, **71** Q4
15 Wang, H.F.: 'Phillips–Heffron model of power systems installed with STATCOM and applications', *IEE Proc. Part C*, 1999, **146**, (5), pp. 521–527
16 Wang, H.F., Swift, F.J.: 'The capability of the static var compensator in damping power system oscillations', *IEE Proc. Part C*, 1996, (4) Q5
17 Klein, M., Roger, G.J., Kundur, P.: 'A fundamental study of inter-area oscillations in power systems', *IEEE Trans. Power Syst.*, 1991, **6**, (3), pp. 914–921
18 Yang, X., Feliachi, A.: 'Stabilization of inter-area oscillation modes through excitation systems', *IEEE Trans. Power Syst.*, 1994, **9**, (1), pp. 494–502
19 Shen, C., Yang, Z., Crow, M.L., Atcitty, S.: 'Control of STATCOM with energy storage device'. IEEE Power Engineering Society Winter Meeting, 2000, 23–27 January 2000, vol. 4, pp. 2722–2728
20 Kunder, P.: 'Power system stability and control' (McGraw-Hill, 1994)

9 Appendix 1

$$v_{sd} = -x_s i_{sq} + kmV_{dc}\cos\psi,\ v_{sq} = x_s i_{sd} + kmV_{dc}\sin\psi$$

By using (18), linearisation of the above equations is

$$\begin{aligned}\Delta v_{sd} &= -x_s\Delta i_{sq} + kV_{dc0}\cos\psi_0\Delta m + km_m\cos\psi_0\Delta V_{dc} \\ &\quad - km_0V_{dc0}\sin\psi_0\Delta\psi \\ &= -x_sb_{21}\Delta\delta - x_sb_{22}\Delta E'_q + (km_m\cos\psi_0 - x_sb_{23})\Delta V_{dc} \\ &\quad + (kV_{dc0}\cos\psi_0 - x_sb_{24})\Delta m \\ &\quad - (km_0V_{dc0}\sin\psi_0 + x_sb_{25})\Delta\psi \\ \Delta v_{sq} &= x_s\Delta i_{sd} + kV_{dc0}\sin\psi_0\Delta m + km_0\sin\psi_0\Delta V_{dc} \\ &\quad + km_0V_{dc0}\cos\psi_0\Delta\psi \\ &= x_sb_{41}\Delta\delta + x_sb_{42}\Delta E'_q + (km_m\sin\psi_0 + x_sb_{43})\Delta V_{dc} \\ &\quad + (kV_{dc0}\sin\psi_0 + x_sb_{44})\Delta m \\ &\quad - (km_0V_{dc0}\cos\psi_0 - x_sb_{45})\Delta\psi \end{aligned} \tag{39}$$

By using (39), we can have

$$\begin{aligned}\Delta V_s &= \left(\frac{V_{sd0}}{V_{s0}}\Delta v_{sd} + \frac{V_{sq0}}{V_{s0}}\Delta v_{sq}\right) = B_1\Delta\delta + B_2\Delta E'_q \\ &\quad + B_{dc}\Delta V_{dc} + B_3\Delta m + B_4\Delta\psi\end{aligned} \tag{40}$$

where

$$\begin{aligned}B_1 &= -\frac{V_{sd0}}{V_{s0}}x_sb_{21} + \frac{V_{sq0}}{V_{s0}}x_sb_{41} \\ B_2 &= -\frac{V_{sd0}}{V_{s0}}x_sb_{22} + \frac{V_{sq0}}{V_{s0}}x_sb_{42} \\ B_{dc} &= \frac{V_{sd0}}{V_{s0}}(km_m\cos\psi_0 - x_sb_{23}) + \frac{V_{sq0}}{V_{s0}}(km_m\sin\psi_0 + x_sb_{43}) \\ B_3 &= \frac{V_{sd0}}{V_{s0}}(kV_{dc0}\cos\psi_0 - x_sb_{24}) + \frac{V_{sq0}}{V_{s0}}(kV_{dc0}\sin\psi_0 + x_sb_{44}) \\ B_4 &= -\frac{V_{sd0}}{V_{s0}}(km_0V_{dc0}\sin\psi_0 + x_sb_{25}) \\ &\quad - \frac{V_{sq0}}{V_{s0}}(km_0V_{dc0}\cos\psi_0 - x_sb_{45})\end{aligned}$$

From Fig. 3 we can have

$$\psi = \phi + \tan^{-1}\frac{v_{sq}}{v_{sd}} \tag{41}$$

By using (39), linearisation of the above equation can be obtained to be

$$\begin{aligned}\Delta\psi &= \Delta\phi + \frac{1}{1 + (v_{sq0}/v_{sd0})^2}\left(\frac{1}{v_{sd0}}\Delta v_{sq} - \frac{v_{sq0}}{v_{sd0}^2}\Delta v_{sd}\right) \\ &= \Delta\phi + \frac{1}{v_{sd0}^2 + v_{sq0}^2}(v_{sd0}\Delta v_{sq} - v_{sq0}\Delta v_{sd}) \\ &= \Delta\phi + g'_1\Delta\delta + g'_2\Delta E'_q + g'_{dc}\Delta V_{dc} + g'_3\Delta m + g'_4\Delta\psi\end{aligned} \tag{42}$$

where

$$\begin{aligned}g'_1 &= \frac{1}{v_{sd0}^2 + v_{sq0}^2}(v_{sd0}x_sb_{41} + v_{sq0}x_sb_{21}) \\ g'_2 &= \frac{1}{v_{sd0}^2 + v_{sq0}^2}(v_{sd0}x_sb_{42} + v_{sq0}x_sb_{22}) \\ g'_{dc} &= \frac{1}{v_{sd0}^2 + v_{sq0}^2}[v_{sd0}(km_m\sin\psi_0 + x_sb_{43}) \\ &\quad - v_{sq0}(km_m\cos\psi_0 - x_sb_{23})] \\ g'_3 &= \frac{1}{v_{sd0}^2 + v_{sq0}^2}[v_{sd0}(kV_{dc0}\sin\psi_0 + x_sb_{44}) \\ &\quad - v_{sq0}(kV_{dc0}\cos\psi_0 - x_sb_{24})] \\ g'_4 &= \frac{1}{v_{sd0}^2 + v_{sq0}^2}[-v_{sd0}(km_0V_{dc0}\cos\psi_0 - x_sb_{45}) \\ &\quad + v_{sq0}(km_0V_{dc0}\sin\psi_0 + x_sb_{25})]\end{aligned}$$

Hence

$$\Delta\psi = g\Delta\phi + g_1\Delta\delta + g_2\Delta E'_q + g_{dc}\Delta V_{dc} + g_3\Delta m \tag{43}$$

where

$$\begin{aligned}g &= \frac{g}{1 - g'_4}, \quad g_1 = \frac{g'_1}{1 - g'_4}, \quad g_2 = \frac{g'_2}{1 - g'_4} \\ g_3 &= \frac{g'_3}{1 - g'_4}, \quad g_{dc} = \frac{g'_{dc}}{1 - g'_4}\end{aligned}$$

10 Appendix 2

Linearisation of (3), (5), (6), (7), (9), (11), (12) and (13) gives

$$\begin{aligned}\Delta I_{fc\text{-}ref} &= -\frac{P_{fc\text{-}ref0}}{V_{fc0}^2}\Delta V_{fc} \\ \Delta I_{fc} &= \frac{1}{1 + T_e s}\Delta I_{fc\text{-}ref} \\ \Delta q_{h2\text{-}in} &= \frac{2K_r}{U_{opt}}\frac{1}{1 + T_f s}\Delta I_{fc} \\ \Delta q_{o2\text{-}in} &= \frac{1}{r_{ho}}\Delta q_{h2\text{-}in} \\ \Delta p_{h2} &= \frac{1}{K_{h2}}\frac{1}{1 + T_{h2}s}(\Delta q_{h2\text{-}in} - 2K_r\Delta I_{fc}) \\ \Delta p_{o2} &= \frac{1}{K_{o2}}\frac{1}{1 + T_{o2}s}(\Delta q_{o2\text{-}in} - K_r\Delta I_{fc}) \\ \Delta p_{h2o} &= \frac{1}{K_{h2o}}\frac{1}{1 + T_{h2o}s}2K_r\Delta I_{fc} \\ \Delta V_{fc} &= c_1\Delta p_{h2} + c_2\Delta p_{o2} + c_3\Delta p_{h2o} + c_4\Delta I_{fc}\end{aligned} \tag{44}$$

$$\Delta d_c = -T_{dc}(s)\Delta I_{fc} \tag{45}$$

doi: 10.1049/iet-rpg.2010.0024

$$\begin{aligned}\Delta I_{\mathrm{dc1}} &= m_0\, k\cos\psi_0\Delta i_{sd} + m_0\, k\sin\psi_0 i_{sq} \\ &\quad + (i_{sd0}k\cos\psi_0 + i_{sq0}k\sin\psi_0)\Delta m \\ &\quad + (i_{sq0}m_0\, k\cos\psi_0 - i_{sd0}m_0\, k\sin\psi_0)\Delta\psi \\ \Delta I_{\mathrm{dc2}} &= (1-d_{c0})\Delta I_{\mathrm{fc}} - I_{\mathrm{fc0}}\Delta d_{\mathrm{c}} \\ \Delta\dot{V}_{\mathrm{dc}} &= \frac{1}{C_{\mathrm{dc}}}(\Delta I_{\mathrm{dc2}} - \Delta I_{\mathrm{dc1}})\end{aligned} \tag{46}$$

Let the state-space realisation of (45) (dc–dc converter control) to be

$$\begin{aligned}\dot{\boldsymbol{X}}_d &= \boldsymbol{A}_d\boldsymbol{X}_d + \boldsymbol{B}_d\Delta I_{\mathrm{fc}} \\ \Delta d_c &= \boldsymbol{C}_d\boldsymbol{X}_d + D_d\Delta I_{\mathrm{fc}}\end{aligned} \tag{47}$$

From (44)–(47) it can be obtained that

$$\begin{aligned}C_{\mathrm{dc}}\Delta\dot{V}_{\mathrm{dc}} &= (1-d_{c0})\Delta I_{\mathrm{fc}} - I_{\mathrm{fc0}}\boldsymbol{C}_d\boldsymbol{X}_d + D_d\Delta I_{\mathrm{fc}} - f_1\Delta i_{sd} \\ &\quad - f_2\psi_0\Delta i_{sq} - f_3\Delta m - f_4\Delta\psi \\ \Delta I_{\mathrm{fc}} &= -\frac{1}{1+T_e s}\frac{P_{\text{fc-ref0}}}{V_{\mathrm{fc0}}^2}(c_1\Delta p_{\mathrm{h2}} + c_2\Delta p_{\mathrm{o2}} \\ &\quad + c_3\Delta p_{\mathrm{h2o}} + c_4\Delta I_{\mathrm{fc}}) \\ \Delta q_{\text{h2-in}} &= \frac{2K_r}{U_{\mathrm{opt}}}\frac{1}{1+T_{\mathrm{f}}s}\Delta I_{\mathrm{fc}} \\ \Delta p_{\mathrm{h2}} &= \frac{1}{K_{\mathrm{h2}}}\frac{1}{1+T_{\mathrm{h2}}s}(\Delta q_{\text{h2-in}} - 2K_r\Delta I_{\mathrm{fc}}) \\ \Delta p_{\mathrm{o2}} &= \frac{1}{K_{\mathrm{o2}}}\frac{1}{1+T_{\mathrm{o2}}s}\left(\frac{1}{r_{\mathrm{ho}}}\Delta q_{\text{h2-in}} - K_r\Delta I_{\mathrm{fc}}\right) \\ \Delta p_{\mathrm{h2o}} &= \frac{1}{K_{\mathrm{h2o}}}\frac{1}{1+T_{\mathrm{h2o}}s}2K_r\Delta I_{\mathrm{fc}} \\ \dot{\boldsymbol{X}}_d &= \boldsymbol{A}_d\boldsymbol{X}_d + \boldsymbol{B}_d\Delta I_{\mathrm{fc}}\end{aligned} \tag{48}$$

where

$$\begin{aligned}f_1 &= m_0\, k\cos\psi_0, f_2 = m_0\, k\sin\psi_0 i_{sq} \\ f_3 &= i_{sd0}k\cos\psi_0 + i_{sq0}k\sin\psi_0 \\ f_4 &= i_{sq0}m_0\, k\cos\psi_0 - i_{sd0}m_0\, k\sin\psi_0\end{aligned}$$

Define the state variable vector of the state-space representation of the above linearised model of SOFC power generation plant to be

$$\boldsymbol{X}_{\mathrm{fc}} = \begin{bmatrix}\Delta V_{\mathrm{dc}} & \Delta I_{\mathrm{fc}} & \Delta q_{\text{h2-in}} & \Delta p_{\mathrm{h2}} & \Delta p_{\mathrm{h2o}} & \Delta p_{\mathrm{o2}} & \boldsymbol{X}_d\end{bmatrix}^{\mathrm{T}}$$

Equation (48) can be written as

$$\dot{\boldsymbol{X}}_{\mathrm{fc}} = \boldsymbol{A}'_{\mathrm{fc}}\boldsymbol{X}_{\mathrm{fc}} + \boldsymbol{B}'_{\mathrm{fc1}}\begin{bmatrix}\Delta i_{sd} & \Delta i_{sq}\end{bmatrix}^{\mathrm{T}} + \boldsymbol{B}'_{\mathrm{fc2}}\begin{bmatrix}\Delta m & \Delta\psi\end{bmatrix}^{\mathrm{T}}$$

where (see equations at the bottom of the page)

11 Appendix 3

From (13) we can have

$$\begin{aligned}V_{\mathrm{dc}}\dot{V}_{\mathrm{dc}} &= \frac{1}{C_{\mathrm{dc}}}I_{\mathrm{dc}} = \frac{1}{C_{\mathrm{dc}}}(V_{\mathrm{dc}}I_{\mathrm{dc2}} - V_{\mathrm{dc}}I_{\mathrm{dc1}}) \\ &= \frac{1}{C_{\mathrm{dc}}}(P_{\mathrm{fc}} - P_{\mathrm{s}})\end{aligned} \tag{49}$$

Hence

$$\begin{aligned}V_{\mathrm{dc0}}\Delta\dot{V}_{\mathrm{dc}} + \Delta\dot{V}_{\mathrm{dc0}}\Delta V_{\mathrm{dc}} &= V_{\mathrm{dc0}}E\dot{V}_{\mathrm{dc}} \\ &= \frac{1}{C_{\mathrm{dc}}}(\Delta P_{\mathrm{fc}} - \Delta P_{\mathrm{s}})\end{aligned} \tag{50}$$

Power balance equation of the power system is $P_{\mathrm{t}} - P_{\mathrm{s}} + P_{\mathrm{a}} = P_m$, where P_{a} is the accelerating power gained by the generator in dynamic operation of the power system. $\Delta P_{\mathrm{t}} = \Delta P_{\mathrm{s}} - \Delta P_{\mathrm{a}}$, that is, in the dynamic operation, ΔP_{s} is in the same phase with ΔP_{t}, lagging $\Delta\omega$ by 90°. From

$$\boldsymbol{A}'_{\mathrm{fc}} = \begin{bmatrix}
0 & \frac{(1-d_{c0})+D_d}{C_{\mathrm{dc}}} & 0 & 0 & 0 & 0 & \frac{-I_{\mathrm{fc0}}\boldsymbol{C}_d}{C_{\mathrm{dc}}} \\
0 & -\frac{1}{T_e} - \frac{1}{T_e}\frac{P_{\text{fc-ref0}}}{V_{\mathrm{fc0}}^2}c_4 & 0 & -\frac{1}{T_e}\frac{P_{\text{fc-ref0}}}{V_{\mathrm{fc0}}^2}c_1 & -\frac{1}{T_e}\frac{P_{\text{fc-ref0}}}{V_{\mathrm{fc0}}^2}c_3 & -\frac{1}{T_e}\frac{P_{\text{fc-ref0}}}{V_{\mathrm{fc0}}^2}c_2 & 0 \\
0 & \frac{2K_r}{U_{\mathrm{opt}}T_{\mathrm{f}}} & -\frac{1}{T_f} & 0 & 0 & 0 & 0 \\
0 & -\frac{2K_r}{K_{\mathrm{h2}}T_{\mathrm{h2}}} & \frac{1}{K_{\mathrm{h2}}T_{\mathrm{h2}}} & -\frac{1}{T_{\mathrm{h2}}} & 0 & 0 & 0 \\
0 & \frac{2K_r}{K_{\mathrm{h2o}}T_{\mathrm{h2o}}} & 0 & 0 & -\frac{1}{T_{\mathrm{h2o}}} & 0 & 0 \\
0 & -\frac{K_r}{K_{\mathrm{o2}}T_{\mathrm{o2}}} & \frac{K_r}{K_{\mathrm{o2}}T_{\mathrm{o2}}r_{\mathrm{ho}}} & 0 & 0 & -\frac{1}{T_{\mathrm{o2}}} & 0 \\
\boldsymbol{0} & \boldsymbol{B}_d & \boldsymbol{0} & \boldsymbol{0} & \boldsymbol{0} & \boldsymbol{0} & \boldsymbol{A}_d
\end{bmatrix}$$

$$\boldsymbol{B}'_{\mathrm{fc1}} = \begin{bmatrix}\frac{-f_1}{C_{\mathrm{dc}}} & \frac{-f_2}{C_{\mathrm{dc}}} \\ \boldsymbol{0} & \boldsymbol{0}\end{bmatrix}, \quad \boldsymbol{B}'_{\mathrm{fc2}} = \begin{bmatrix}\frac{-f_3}{C_{\mathrm{dc}}} & \frac{-f_4}{C_{\mathrm{dc}}} \\ \boldsymbol{0} & \boldsymbol{0}\end{bmatrix}$$

(50) it can be seen that ΔV_{dc} which is caused by ΔP_s should lead ΔP_s by 90°. Therefore ΔV_{dc} is in the same phase with $\Delta\omega$.

12 Appendix 4

From (30), the active power supplied by the generator can be written as

$$\begin{aligned}P_t &= \frac{E'_q}{x'_{d\Sigma}}(bV_b\sin\delta + aV_c\cos\psi)\\ &\quad -\frac{(x_q - x'_d)}{x'_{d\Sigma}x_{q\Sigma}}(bV_b\sin\delta + aV_c\cos\psi)(bV_b\cos\delta + aV_c\sin\psi)\\ &= \frac{E'_q}{x'_{d\Sigma}}(bV_b\sin\delta + aV_c\cos\psi)\\ &\quad -\frac{(x_q - x'_d)}{x'_{d\Sigma}x_{q\Sigma}}\Big[b^2V_b^2\sin\delta\cos\delta + baV_cV_b\sin\delta\sin\psi\\ &\quad + abV_bV_c\cos\psi\cos\delta + \frac{1}{2}a^2V_c^2\sin 2\psi\Big]\end{aligned}$$

where $V_c = mkV_{dc}$, $\Delta\psi = K_{vdc}\Delta V_{dc}$. Hence

$$\begin{aligned}\Delta T_{DDET} &= \frac{\partial P_t}{\partial V_{dc}} + \frac{\partial P_t}{\partial V_{dc}}R\\ &= \frac{amkE'_{q0}}{x'_{d\Sigma}}(\cos\psi_0 - RV_{dc0}\sin\psi_0)\\ &\quad -\frac{(x_q - x'_d)}{x'_{d\Sigma}x_{q\Sigma}}[mkabV_{b0}\sin\delta_0(RV_{dc0}\cos\psi_0 + \sin\psi_0)\\ &\quad + amkbV_{b0}\cos\delta_0(\cos\psi_0 - RV_{dc0}\sin\psi_0)\\ &\quad + m^2k^2a^2V_{dc0}(\sin 2\psi_0 + RV_{dc0}\cos 2\psi_0)]\\ &= 0\end{aligned} \tag{51}$$

By solving (51), the accurate value of $\psi_{0\text{-critical}}$ can be computed.

13 Appendix 5

Per unit values of the following parameters are used, including for the relevant dc-system in the examples.

1. Parameters of the example single-machine infinite-bus power system (machine damping coefficient includes the effect of a PSS. A relatively low gain AVR is adopted.)

Transmission line: $x_{ts} = 0.3$ p.u., $x_{sb} = 0.3$ p.u., $x_s = 0.3$ p.u., Generator: $x_d = 1.3$ p.u., $x_q = 0.47$ p.u., $x'_d = 0.3$ p.u., $M = 7.4$ s, $D = 4$ p.u., $T'_{d0} = 5$ s

AVR: $T_A = 0.1$ s, $K_A = 10$ p.u.

Initial load condition: $V_{t0} = 1.0$ p.u., $V_{s0} = 1.0$ p.u., $V_{b0} = 1.0$ p.u.

Converters (voltage control scheme)

$$m = m_0 + \left(K_{vac} + \frac{K_{vaci}}{s}\right)(V_{s\text{-ref}} - V_s)$$

$$\phi = \phi_0 + K_{vdc} + \frac{K_{vdci}}{s})(V_{dc\text{-ref}} - V_{dc})$$

$C_{dc} = 1.0$ p.u., $V_{dc0} = 1.0$ p.u., $K_{vac} = 0.1$, $K_{vaci} = 0.3$, $K_{vdc} = 0.3$, $K_{vdci} = 0.3$, $K_{dc} = 5$

2. Parameters of the example four-machine two-area power system

DC/DC inverter: $d_c = d_{c0} + (K_{fc} + (K_{fci}/s))(I_{fc\text{-ref}} - I_{fc})$; $K_{fc} = 3$; $K_{fci} = 1.57$

DC/AC converter (current control scheme)

$$m = m_0 + K_r(s)[I_{sq0} - I_{sq} + K_{ac}(s)(V_{s\text{-ref}} - V_s)]$$

$$\phi = \phi_0 + K_a(s)[I_{sq0} - I_{sq} + K_{dc}(s)(V_{dc\text{-ref}} - V_{dc})]$$

$$K_{dc}(s) = K_{dcp} + K_{dci}/s\ K_{ac}(s) = K_{acp} + K_{aci}/s$$

$$K_r(s) = K_{rp} + K_{ri}/s\ K_a(s) = K_{ap} + K_{ai}/s$$

$$K_{dcp} = 0.2;\ K_{dci} = 2;\ K_{acp} = 0.15;\ K_{aci} = 0.0001$$

$$K_{rp} = -0.001;\ K_{ri} = -0.001$$

$$K_{ap} = 0.001;\ K_{ai} = 0.001;$$

Parameters of the example system are given in [20] with parameters of the AVR for four generators to be $K_A = 100$; $T_A = 0.01$;

3. Parameters of the SOFC:

$$\text{SOFC: } T = 1273,\ F = 96487,\ R = 8.314,\ E0 = 1.18$$

$$N0 = 384,\ K_r = 0.966e-6,\ U_{max} = 0.9,\ U_{min} = 0.8,$$

$$U_{opt} = 0.85,\ K_{h2} = 8.43 \times 10^{-4},\ K_{h2o} = 2.81e-4$$

$$K_{o2} = 2.52 \times 10^{-3},\ t_{h2} = 26.1,\ t_{h2o} = 78.3$$

$$t_{o2} = 2.91,\ r = 0.126,\ T_f = 5,\ T_e = 0.08$$

$$r_{ho} = 1.145$$

doi: 10.1049/iet-rpg.2010.0024

RPG20100024

Author Queries

W. Du, H.F. Wang, X.F. Zhang, L.Y. Xiao

Q1 Please check the corresponding author e-mail id.
Q2 Please provide subcaption for Fig. 3.
Q3 Please provide author group in ref. [11].
Q4 Kindly provide page range in ref. [14].
Q5 Please provide volume and page range in ref. [16]
Q6 Please expand AVR at the first occurrence.